J|A|C|S ARTICLES

Published on Web 11/04/2009

Mechanistic Insights into Hydride-Transfer and Electron-Transfer Reactions by a Manganese(IV)−Oxo Porphyrin Complex

Shunichi Fukuzumi,*[,†,‡] Naofumi Fujioka,[†] Hiroaki Kotani,[†] Kei Ohkubo,[†] Yong-Min Lee,[‡,§] and Wonwoo Nam*[,‡,§]

Department of Material and Life Science, Graduate School of Engineering, Osaka University, SORST, Japan Science and Technology Agency (JST), Suita, Osaka 565-0871, Japan, Department of Bioinspired Science, Ewha Womans University, Seoul 120-750, Korea, and Department of Chemistry and Nano Science, Center for Biomimetic Systems, Ewha Womans University, Seoul 120-750, Korea

Received June 4, 2009; E-mail: fukuzumi@chem.eng.osaka-u.ac.jp; wwnam@ewha.ac.kr

Abstract: Hydride transfer from dihydronicotinamide adenine dinucleotide (NADH) analogs to a manganese(IV)−oxo porphyrin complex, (TMP)Mn^{IV}(O) [TMP = 5,10,15,20-tetrakis(2,4,6-trimethylphenyl)porphyrin], occurs via disproportionation of (TMP)Mn^{IV}(O) to [(TMP)Mn^{III}]$^+$ and [(TMP)Mn^{V}(O)]$^+$ that acts as the actual hydride acceptor. In contrast, electron transfer from ferrocene derivatives to (TMP)Mn^{IV}(O) occurs directly to afford ferricenium ions and (TMP)Mn^{III}(OH) products. The disproportionation rate constant of (TMP)Mn^{IV}(O) was determined by the dependence of the observed second-order rate constants on concentrations of NADH analogs to be (8.0 ± 0.6) × 10^6 M^{-1} s^{-1} in acetonitrile at 298 K. The disproportionation rate constant of (TMP)Mn^{IV}(O) in hydride-transfer reactions increases linearly with increasing acid concentration, whereas the rate constant of electron transfer from ferrocene to (TMP)Mn^{IV}(O) remains constant irrespective of the acid concentration. The rate constants of electron transfer from a series of ferrocene derivatives to (TMP)Mn^{IV}(O) were evaluated in light of the Marcus theory of electron transfer to determine the reorganization energy of electron transfer by the (TMP)Mn^{IV}(O) complex.

Introduction

An important objective in studying biological oxidation reactions is to elucidate structures of reactive intermediates and mechanisms of oxygen atom transfer reactions by the intermediates occurring at the active sites of enzymes.[1] Since high-valent metal-oxo species have been implicated as the key reactive intermediates in various oxidation reactions, a number of biomimetic metal-oxo complexes have been synthesized, characterized spectroscopically, and used as oxidants in mechanistic studies of oxidation reactions.[1,2] A notable example is the high-valent iron(IV)−oxo porphyrin π-cation radical species, [(Porp)$^{+\bullet}$$Fe^{IV}$=O]$^+$ (Porp = porphinato dianion), proposed as active oxidants in the catalytic cycles of cytochromes P450.[3] Another high-valent metal−oxo species that has attracted much attention in biomimetic oxidation reactions is manganese-oxo porphyrins, [(Porp)Mn^{V}(O)]$^+$ and (Porp)Mn^{IV}(O), since high-valent manganese-oxo intermediates are thought to play key roles with high reactivities in useful oxidation reactions and in the production of dioxygen at the oxygen-evolving center of photosystem II.[4,5]

Very recently, Mn(V)−oxo porphyrins were characterized with various spectroscopic techniques, such as UV−vis, ^{1}H NMR, EPR, resonance Raman, and X-ray absorption spectroscopy/extended X-ray absorption fine structure spectroscopy (XAS/EXAFS) in aqueous or organic solvents.[6−8] Reactivities of the Mn(V)−oxo porphyrins have also been investigated in various oxidation reactions, including olefin epoxidation, C−H activation and hydride-transfer reactions, and the oxidation of halides, sulfides, PR_3, and NR_3, as well as in theoretical calculations.[6−11] In contrast to the Mn(V)−oxo porphyrin complexes, Mn(IV)−oxo porphyrins have been rarely used as an oxidant in oxidation reactions due to the low oxidizing power

[†] Osaka University, SORST, JST.
[‡] Department of Bioinspired Science, Ewha Womans University.
[§] Center for Biomimetic Systems, Ewha Womans University.

(1) Nam, W. *Acc. Chem. Res.* **2007**, *40*, 465 and review articles in the special issue.
(2) *Metal-Oxo and Metal-Peroxo Species in Catalytic Oxidations*; Meunier, B., Ed.; Springer-Verlag: Berlin, 2000.
(3) (a) van Eldik, R. *Coord. Chem. Rev.* **2007**, *251*, 1649–1662. (b) Nam, W. *Acc. Chem. Res.* **2007**, *40*, 522–531. (c) Shaik, S.; Hirao, H.; Kumar, D. *Acc. Chem. Res.* **2007**, *40*, 532–542. (d) Makris, T. M.; von Koenig, K.; Schlichting, I.; Sligar, S. G. *J. Inorg. Biochem.* **2006**, *100*, 507–518. (e) Ortiz. de Montellano, P. R. *Cytochrome P450: Structure, Mechanism, and Biochemistry*, 3rd ed.; Kluwer Academic/Plenum Publishers: New York, 2005. (f) Denisov, I. G.; Makris, T. M.; Sligar, S. G.; Schlichting, I. *Chem. Rev.* **2005**, *105*, 2253–2278. (g) Shaik, S.; Kumar, D.; de Visser, S. P.; Altun, A.; Thiel, W. *Chem. Rev.* **2005**, *105*, 2279–2328. (h) Meunier, B.; de Visser, S. P.; Shaik, S. *Chem. Rev.* **2004**, *104*, 3947–3980. (i) Groves, J. T *Proc. Natl. Acad. Sci. U.S.A.* **2003**, *100*, 3569–3574.
(4) (a) Meunier, B. *Chem. Rev.* **1992**, *92*, 1411–1456. (b) Mansuy, D. *Coord. Chem. Rev.* **1993**, *125*, 129–141. (c) Meunier, B.; Robert, A.; Pratviel, G.; Bernadou, J. In *The Porphyrin Handbook*; Kadish, K. M., Smith, K. M., Guilard, R., Eds.; Academic Press: San Diego, 2000; Vol. 4, Chapter 31, pp 119−187. (d) Groves, J. T. In *Cytochrome P450: Structure, Mechanism, and Biochemistry*, 3rd ed; Ortiz de Montellano, P. R., Ed.; Kluwer Academic/Plenum Publishers: New York, 2005; pp 1−43.
(5) (a) Betley, T. A.; Wu, Q.; Voorhis, T. V.; Nocera, D. G. *Inorg. Chem.* **2008**, *47*, 1849–1861. (b) Mullins, C.; Pecoraro, V. L. *Coord. Chem. Rev.* **2008**, *252*, 416–443. (c) Cady, C. W.; Crabtree, R. H.; Brudvig, G. W. *Coord. Chem. Rev.* **2008**, *252*, 444–455. (d) McEvoy, J. P.; Brudvig, G. W. *Chem. Rev.* **2006**, *106*, 4455–4483. (e) Wydrzynski, T. *Photosystem II: The Light-Driven Water: Plastoquinone Oxidoreductase*; Springer: New York, 2005.

Scheme 1

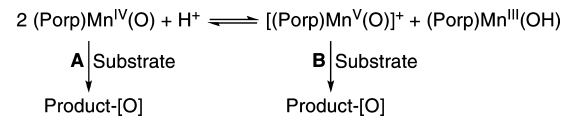

in nature. However, Newcomb and co-workers reported recently that Mn(IV)−oxo complexes are capable of oxygenating Ph_3P, Ph_3N, and *cis*-stilbene in organic solvents.[12,13] In the study, (Porp)Mn^{IV}(O) has been shown to react with substrates to give [(Porp)Mn^{III}]$^+$ and oxygenated products, but the formation of (Porp)Mn^{II} species was not observed.[12] On the basis of the inverted reactivity of (Porp)Mn^{IV}(O) bearing different porphyrin ligand, the authors proposed that [(Porp)Mn^{V}(O)]$^+$, produced by the disproportionation of (Porp)Mn^{IV}(O), is the actual oxidant responsible for the oxidation of organic substrates (Scheme 1, pathway B).[12] However, the second-order kinetics for the disproportionation of (Porp)Mn^{IV}(O) to produce [(Porp)Mn^{III}]$^+$ and [(Porp)Mn^{V}(O)]$^+$ have yet to be directly observed, although the disproportionation rate constants for (TPP)Mn^{IV}(O) (TPP = 5,10,15,20-tetraphenylporphyrin) and (TPFPP)Mn^{IV}(O) (TPFPP = 5,10,15,20-tetrakis(pentafluorophenyl)porphyrin) were estimated to be 3×10^9 and 1×10^6 M^{-1} s^{-1}, respectively.[12] Further, there are two possible pathways for the reactions of (Porp)Mn^{IV}(O) with substrates: the direct oxidation of substrates by (Porp)Mn^{IV}(O) (Scheme 1, pathway A) and the oxidation of substrates by [(Porp)Mn^{V}(O)]$^+$ formed from (Porp)Mn^{IV}(O) via the disproportionation equilibrium (Scheme 1, pathway B).[12,13] Thus, the reaction pathway may vary depending on the substrates and/or reaction types, and it is of interest to understand factors that control the reaction pathways of (Porp)Mn^{IV}(O) in oxidation reactions.

We report herein the first direct evidence for the disproportionation of (TMP)Mn^{IV}(O) [TMP = 5,10,15,20-tetrakis(2,4,6-trimethylphenyl)porphyrin] to [(TMP)Mn^{III}]$^+$ and [(TMP)Mn^{V}(O)]$^+$ that is the true oxidant in hydride transfer from a series of dihydronicotinamide adenine dinucleotide (NADH) analogs to (TMP)Mn^{IV}(O); the disproportionation of (TMP)Mn^{IV}(O) to (TMP)Mn^{III}X and [(TMP)Mn^{V}(O)]$^+$ turned out to be the rate-determining step, and the second-order rate constants were determined in the hydride-transfer reactions. In contrast to the hydride-transfer reactions, rates of electron transfer from a series of ferrocene derivatives to (TMP)Mn^{IV}(O) obeyed pseudofirst-order kinetics. The kinetic comparison between the hydride-transfer and electron-transfer reactions of (TMP)Mn^{IV}(O) enables us to distinguish two different reaction pathways occurring by one common oxidant: Hydride transfer from NADH analogs to (TMP)Mn^{IV}(O) occurs by the formation of [(TMP)Mn^{V}(O)]$^+$ via the disproportionation pathway, whereas direct electron transfer from ferrocene derivatives to (TMP)Mn^{IV}(O) occurs in the electron transfer reaction. In addition, driving force dependence of rate constants of electron transfer from a series of ferrocene derivatives to (TMP)Mn^{IV}(O) is analyzed in light of the Marcus theory of electron transfer,[14] leading us to determine the reorganization energy of electron transfer of (TMP)Mn^{IV}(O). The latter result provides an excellent opportunity to compare the reactivities in hydride-transfer reactions and the reorganization energies in electron-transfer reactions by a manganese(IV)−oxo porphyrin and nonheme iron(IV)−oxo complexes.[15] The investigated compounds in this study are presented in Chart 1.

Experimental Section

Materials. Commercially available reagents, 10-methylacridone, acridine, methyl iodide (MeI), $NaBH_4$, 5,10,15,20-tetrakis(2,4,6-trimethylphenyl)porphyrin (TMP), and ferrocene (Tokyo Chemical Industry Co., Ltd.), dimethylferrocene (Aldrich Chemical Co.), 1-bromoferrocene (Alfa Aesar GmbH & Co. KG), and $LiAlD_4$ and $NaBD_4$ (CIL, Inc.), were the best available purity and used without further purification unless otherwise noted. Acetonitrile (MeCN) and ether were dried according to the literature procedures and distilled under Ar prior to use.[16] *m*-Chloroperbenzoic acid (*m*-CPBA) was purified by washing with phosphate buffer (pH 7.4) followed by water and then dried under reduced pressure.[17] 9,10-Dihydro-10-methylacridine ($AcrH_2$) was prepared from 10-methylacridinium iodide ($AcrH^+I^-$) by reduction with $NaBH_4$ in methanol and purified by recrystallization from ethanol.[18] $AcrH^+I^-$ was prepared by the reaction of acridine with methyl iodide in acetone and was converted to the perchlorate salt ($AcrH^+ClO_4^-$) by the addition of magnesium perchlorate to the iodide salt ($AcrH^+I^-$) and purified by recrystallization from methanol.[18] The dideuterated compound, [9,9′-$^2H_2$]-10-methylacridine ($AcrD_2$), was prepared from 10-methylacridone by reduction with $LiAlD_4$ in ether.[18] 9-Phenyl-9,10-dihydro-10-methylacridine (AcrHPh) and 9-methyl-9,10-dihydro-10-methylacridine (AcrHMe) were prepared by the reduction of $AcrH^+I^-$ with the corresponding Grignard reagents (PhMgBr or MeMgBr).[19] 9-Phenyl-10-methylacridinium perchlorate ($AcrR^+ClO_4^-$: R = Me and Ph) was prepared by the reaction of 10-methylacridone in dichloromethane with the corresponding Grignard reagents (RMgX) and purified by recrystallization from ethanol-diethyl ether.[20] (TMP)Mn^{III}(Cl) was prepared by adding

(6) (a) Groves, J. T.; Watanabe, Y.; McMurry, T. J. *J. Am. Chem. Soc.* **1983**, *105*, 4489–4490. (b) Groves, J. T.; Lee, J.; Marla, S. S. *J. Am. Chem. Soc.* **1997**, *119*, 6269–6273. (c) Jin, N.; Groves, J. T. *J. Am. Chem. Soc.* **1999**, *121*, 2923–2924. (d) Jin, N.; Ibrahim, M.; Spiro, T. G.; Groves, J. T. *J. Am. Chem. Soc.* **2007**, *129*, 12416–12417. (e) Gross, Z. *Angew. Chem., Int. Ed.* **2008**, *47*, 2737–2739.
(7) (a) Nam, W.; Kim, I.; Lim, M. H.; Choi, H. J.; Lee, J. S.; Jang, H. G. *Chem.—Eur. J.* **2002**, *8*, 2067–2071. (b) Song, W. J.; Seo, M. S.; George, S. D.; Ohta, T.; Song, R.; Kang, M.-J.; Tosha, T.; Kitagawa, T.; Solomon, E. I.; Nam, W. *J. Am. Chem. Soc.* **2007**, *129*, 1268–1277. (c) Lee, J. Y.; Lee, Y.-M.; Kotani, H.; Nam, W.; Fukuzumi, S. *Chem. Commun.* **2009**, 704–706.
(8) Shimazaki, Y.; Nagano, T.; Takesue, H.; Ye, B.-H.; Tani, F.; Naruta, Y. *Angew. Chem., Int. Ed.* **2004**, *43*, 98–100.
(9) (a) Balcells, D.; Raynaud, C.; Crabtree, R. H.; Eisenstein, O. *Chem. Commun.* **2008**, 1772–1774. (b) Balcells, D.; Raynaud, C.; Crabtree, R. H.; Eisenstein, O. *Chem. Commun.* **2008**, 744–746. (c) De Angelis, F.; Jin, N.; Car, R.; Groves, J. T. *Inorg. Chem.* **2006**, *45*, 4268–4276. (d) de Visser, S. P.; Ogliaro, F.; Gross, Z.; Shaik, S. *Chem.—Eur. J.* **2001**, *7*, 4954–4960.
(10) (a) Lahaye, D.; Groves, J. T. *J. Inorg. Biochem.* **2007**, *101*, 1786–1797. (b) Jin, N.; Bourassa, J. L.; Tizio, S. C.; Groves, J. T. *Angew. Chem., Int. Ed.* **2000**, *39*, 3849–3851.
(11) Lee, R. W.; Nakagaki, P. C.; Bruice, T. C. *J. Am. Chem. Soc.* **1989**, *111*, 1368–1372.
(12) Zhang, R.; Horner, J. H.; Newcomb, M. *J. Am. Chem. Soc.* **2005**, *127*, 6573–6582.
(13) (a) Zhang, R.; Newcomb, M. *Acc. Chem. Res.* **2008**, *41*, 468–477. (b) Zhengzheng, P.; Newcomb, M. *Inorg. Chem.* **2007**, *46*, 6767–6774. (c) Zhang, R.; Harischandra, D. N.; Newcomb, M. *Chem.—Eur. J.* **2005**, *11*, 5713–5720. (d) Zhang, R.; Newcomb, M. *J. Am. Chem. Soc.* **2003**, *125*, 12418–12419.
(14) (a) Marcus, R. A. *Annu. Rev. Phys. Chem.* **1964**, *15*, 155–196. (b) Marcus, R. A. *Angew. Chem., Int. Ed.* **1993**, *32*, 1111–1121.
(15) (a) Lee, Y.-M.; Kotani, H.; Suenobu, T.; Nam, W.; Fukuzumi, S. *J. Am. Chem. Soc.* **2008**, *130*, 434–435. (b) Fukuzumi, S.; Kotani, H.; Lee, Y.-M.; Nam, W. *J. Am. Chem. Soc.* **2008**, *130*, 15134–15142.
(16) Armarego, W. L. F.; Chai, C. L. L. *Purification of Laboratory Chemicals*, 5th ed.; Butterworth Heinemann: Amsterdam, 2003.
(17) Bortolini, O.; Campestrini, S.; Di Furia, F.; Modena, G. *J. Org. Chem.* **1987**, *52*, 5093–5095.
(18) Fukuzumi, S.; Koumitsu, S.; Hironaka, K.; Tanaka, T. *J. Am. Chem. Soc.* **1987**, *109*, 305–316.
(19) Fukuzumi, S.; Tokuda, Y.; Kitano, T.; Okamoto, T.; Otera, J. *J. Am. Chem. Soc.* **1993**, *115*, 8960–8968.
(20) Fukuzumi, S.; Ohkubo, K.; Tokuda, Y.; Suenobu, T. *J. Am. Chem. Soc.* **2000**, *122*, 4286–4294.

Chart 1

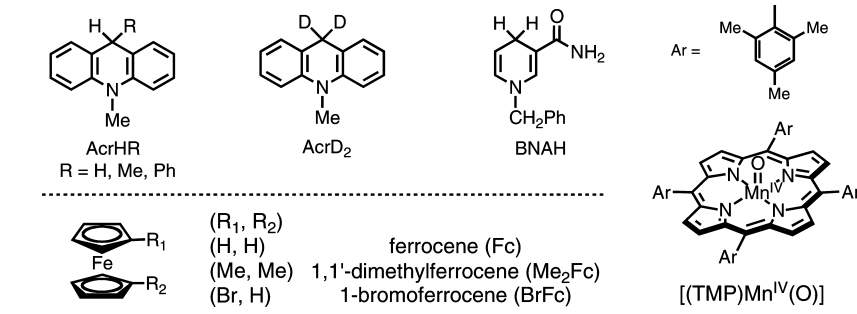

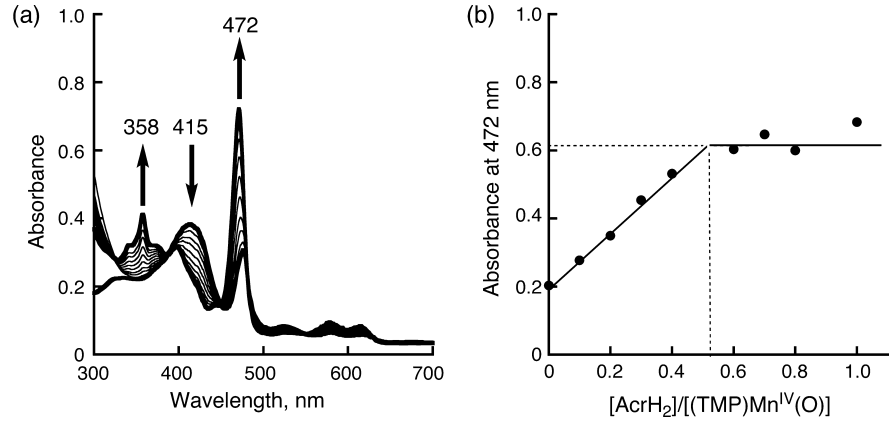

Figure 1. (a) Spectral changes in the reaction of $AcrH_2$ (5.0×10^{-5} M) with [(TMP)Mn^{IV}(O)] (5.0×10^{-6} M) in MeCN at 298 K. (b) Spectral titration of the stoichiometry of the hydride-transfer reactions. (Absorbance at 472 nm vs ratio of [$AcrH_2$] to [(TMP)Mn^{IV}(O)].)

$MnCl_2 \cdot 4H_2O$ to TMP, followed by reflux for 24 h in DMF and wash with HCl, according to the literature method.[21]

Spectral and Kinetic Measurements. Hydride transfer from $AcrH_2$ to (TMP)Mn^{IV}(O) (5.0×10^{-6} M) was examined by monitoring spectral changes in the presence of appropriate amounts of $AcrH_2$ (5.0×10^{-5}–2.0×10^{-4} M) at 298 K, with a Hewlett-Packard 8453 photodiode-array spectrophotometer and a quartz cuvette (path length = 10 mm). Typically, a deaerated MeCN solution of $AcrH_2$ was added with a microsyringe to a deaerated MeCN solution containing (TMP)Mn^{IV}(O) (5.0×10^{-6} M). (TMP)Mn^{IV}(O) was prepared by reacting (TMP)Mn^{III}(Cl) (5.0×10^{-6} M) with 10 equiv of *m*-chloroperbenzoic acid (*m*-CPBA) in MeCN. Subsequently, appropriate amounts of substrates were added to the reaction solutions. Kinetic measurements were performed on a UNISOKU RSP-601 stopped-flow spectrometer equipped with a MOS-type highly sensitive photodiode array or a Hewlett-Packard 8453 photodiode-array spectrophotometer at 298 K. Rates of hydride transfer from $AcrH_2$ to (TMP)Mn^{IV}(O) were monitored by the increases and decrease of absorption bands due to $AcrH^+$ (λ_{max} = 358 nm, $\varepsilon_{max} = 1.8 \times 10^4$ M^{-1} cm^{-1}),[22,23] (TMP)Mn^{III}(OH) (λ_{max} = 472 nm, $\varepsilon_{max} = 1.2 \times 10^5$ M^{-1} cm^{-1}) and (TMP)Mn^{IV}(O) at λ_{max} = 415 nm. The concentration of $AcrH_2$ was maintained to be more than 10-fold excess of the manganese porphyrin reactant. The second-order rate constants were determined by a least-squares curve fit of the second-order plot ($[AcrH^+]^{-1}$ vs time). The second-order plots were linear for three or more half-lives with the correlation coefficient $\rho > 0.999$. In each case, it was confirmed that the rate constants derived from at least five independent measurements agreed within an experimental error of ±5%. Similarly, rates of electron transfer from ferrocene derivatives to (TMP)Mn^{IV}(O) were monitored by the increase and decrease of absorption bands due to (TMP)Mn^{III}(OH) and (TMP)Mn^{IV}(O).

Results and Discussion

Hydride Transfer from NADH Analogs to (TMP)Mn^{IV}(O). (TMP)Mn^{IV}(O) was prepared by the reaction of (TMP)Mn^{III}(Cl) (1.0×10^{-5} M) with *m*-CPBA (5.0×10^{-5} M) according to the literature (see Supporting Information (SI), Figure S1).[24] The formation of (TMP)Mn^{IV}(O) was confirmed by taking an ESR spectrum that agrees well with that reported in the literature (SI, Figure S2).[24] Upon addition of NADH analogs to the solution of (TMP)Mn^{IV}(O), the intermediate reverted back to the starting $[(TMP)Mn^{III}]^+$ complex. The visible spectral changes in oxidation of an NADH analog ($AcrH_2$) by (TMP)Mn^{IV}(O) are shown in Figure 1a, where the absorption band at 415 nm due to (TMP)Mn^{IV}(O) decreases, accompanied by an increase in the absorption band at 358 nm due to 10-methylacridinium ion ($AcrH^+$) and the absorption bands at 472 nm due to (TMP)Mn^{III}(OH). The spectral titration shown in Figure 1b indicates that two equivalents of (TMP)Mn^{IV}(O) oxidize one $AcrH_2$ molecule to produce an $AcrH^+$ ion (eq 1).

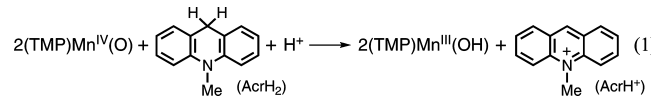

The formation rate of (TMP)Mn^{III}(OH) was determined from an increase in absorbance at 472 nm using a stopped

(21) Rachford, A. A.; Petersen, J. L.; Rack, J. J. *Inorg. Chem.* **2005**, *44*, 8065–8075.
(22) Fukuzumi, S.; Mochizuki, S.; Tanaka, T. *Inorg. Chem.* **1989**, *28*, 2459–2465.
(23) Fukuzumi, S.; Okamoto, K.; Gros, C. P.; Guilard, R. *J. Am. Chem. Soc.* **2004**, *126*, 10441–10449.
(24) (a) Czernuszewicz, R. S.; Su, Y. O.; Stern, M. K.; Macor, K. A.; Kim, D.; Groves, J. T.; Thomas, G.; Spiro, T. G. *J. Am. Chem. Soc.* **1988**, *110*, 4158–4165. (b) Groves, J. T.; Stern, M. K. *J. Am. Chem. Soc.* **1988**, *110*, 8628–8638.

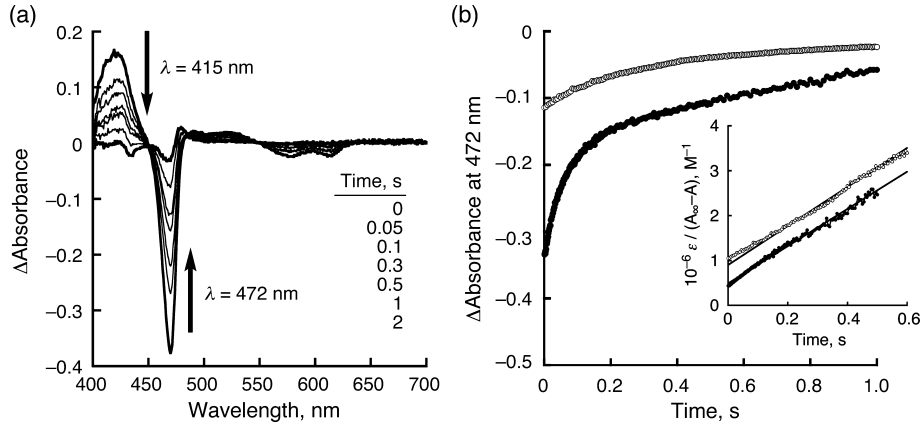

Figure 2. (a) UV−vis spectral changes observed in the oxidation of $AcrH_2$ (5.0×10^{-3} M) by $(TMP)Mn^{IV}(O)$ (5.0×10^{-6} M) in MeCN at 298 K. Note that the different spectra were taken in reference to that after the reaction. (b) Time profile of the absorbance at 472 nm due to $(TMP)Mn^{III}(OH)$ (●, 5.0×10^{-6} M and ○, 1.5×10^{-6} M). (Inset) Second-order plot.

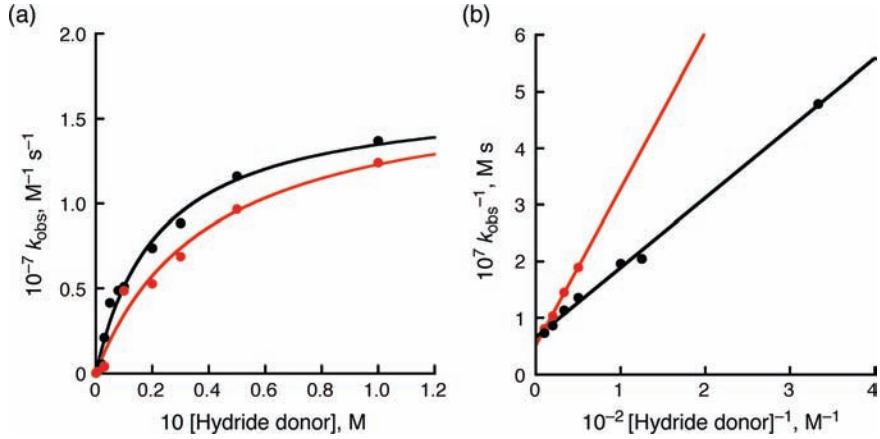

Figure 3. (a) Plots of the observed second-order rate constant (k_{obs}) of hydride transfer from hydride donors to $(TMP)Mn^{IV}(O)$. (b) Plots of k_{obs}^{-1} vs $[Hydride\ donor]^{-1}$ in MeCN at 298 K. Black and red lines are for the reactions of $AcrH_2$ and $AcrD_2$, respectively.

Scheme 2

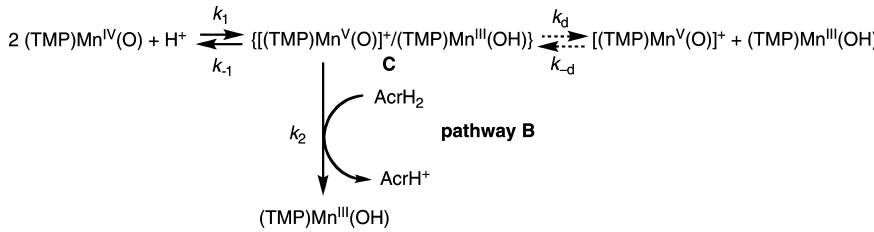

flow technique, coinciding with the decay rate of (TMP)-$Mn^{IV}(O)$ determined from a decrease in absorbance at 415 nm (Figure 2a). The rate obeys second-order kinetics even in the presence of large excess $AcrH_2$, as shown in linear second-order plots shown in the inset of Figure 2b, where the slope that affords the second-order rate constant (k_{obs}) is confirmed to be the same with different initial concentrations of $(TMP)Mn^{IV}(O)$. The k_{obs} value was determined to be $(4.2 \pm 0.3) \times 10^6\ M^{-1}\ s^{-1}$. The observed second-order rate constant (k_{obs}) increases with increasing concentration of $AcrH_2$ to reach a constant value $[(1.6 \pm 0.1) \times 10^7\ M^{-1}\ s^{-1}]$ (Figure 3a). When $AcrH_2$ is replaced by the 9,9′-dideuterated compound ($AcrD_2$), the kinetic deuterium isotope effect is observed at low concentrations ($k_H/k_D = 2.3 \pm 0.1$), but the plateau value exhibits no kinetic deuterium isotope effect (Figure 3a). Such second-order kinetics together with the saturation behavior of the plot of k_{obs} vs $[AcrH_2]$ and the absence of the kinetic deuterium isotope effect can be well explained by the disproportionation of $(TMP)Mn^{IV}(O)$ to afford $[(TMP)Mn^{V}(O)]^+$, which is an actual hydride acceptor, as shown in Scheme 2.

According to Scheme 2, the rate of formation of (TMP)-$Mn^{III}(OH)$ is given by eq 2,

$$d[(TMP)Mn^{III}(OH)]/dt = k_2[C][AcrH_2] + k_1[(TMP)Mn^{IV}(O)]^2 - k_{-1}[C] \quad (2)$$

where C is a pair of $[(TMP)Mn^{V}(O)]^+$ and $(TMP)Mn^{III}(OH)$, which is the same as C in Scheme 2, produced by the comproportionation. The formation rate of C is given by eq 3. Since no $[(TMP)Mn^{V}(O)]^+$ was observed, the rate of comproportionation between $[(TMP)Mn^{V}(O)]^+$ and $(TMP)Mn^{III}(OH)$ may be much faster that the rate of disproportionation. In such a case, a pair C goes back to the reactant pair and reacts with

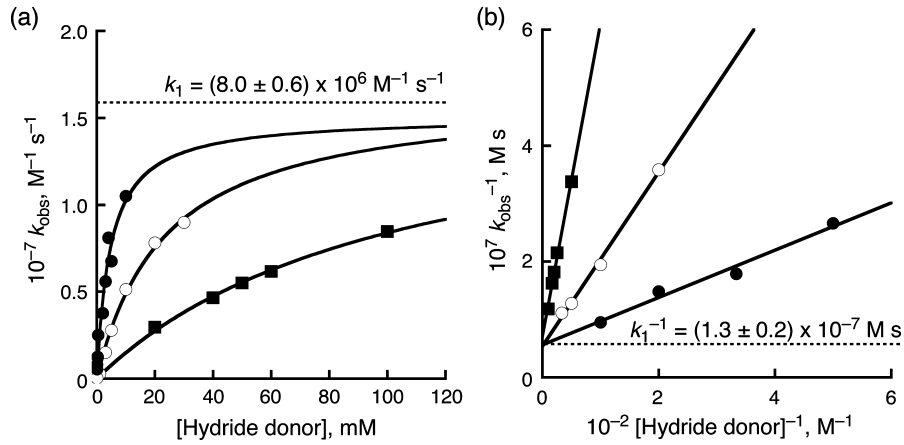

Figure 4. (a) Plots of the observed second-order rate constant (k_{obs}) of hydride transfer from hydride donors to (TMP)Mn^{IV}(O). (b) Plots of k_{obs}^{-1} vs [Hydride donor]$^{-1}$ in MeCN at 298 K (■, AcrHPh; ○, AcrHMe; ●, BNAH).

$AcrH_2$ before dissociation from the solvent cage (k_d) in Scheme 2. Under such conditions that the dissociation rate constant (k_d) is much smaller than k_{-1} and k_2[$AcrH_2$], the rate of formation of C is much faster than the disappearance rate, when the steady state is obtained immediately after starting the reaction: d[C]/dt ≅ 0. Thus, eq 4 is derived by applying the steady-state approximation. Then, eq 5 that fits experimental data is derived by simply combining eqs 2 and 4 (see the detailed derivation in Supporting Information S3),

$$d[C]/dt = k_1[(TMP)Mn^{IV}(O)]^2 - k_{-1}[C] - k_2[C][AcrH_2] \quad (3)$$

$$[C] = k_1[(TMP)Mn^{IV}(O)]^2/(k_{-1} + k_2[AcrH_2]) \quad (4)$$

$$d[(TMP)Mn^{III}(OH)]/dt = 2k_1k_2[(TMP)Mn^{IV}(O)]^2[AcrH_2]/(k_{-1} + k_2[AcrH_2]) \quad (5)$$

indicating that the rate of formation of (TMP)Mn^{III}(OH) obeys second-order kinetics even in the presence of large excess $AcrH_2$ as observed in Figure 3b. The observed second-order rate constant (k_{obs}) is given by eq 6 that can be converted to a linear correlation between k_{obs}^{-1} and [$AcrH_2$]$^{-1}$ (eq 7). Such a linear correlation is confirmed in a linear plot of k_{obs}^{-1} vs [$AcrH_2$]$^{-1}$ in Figure 3b.

$$k_{obs} = 2k_1k_2[AcrH_2]/(k_{-1} + k_2[AcrH_2]) \quad (6)$$

$$k_{obs}^{-1} = (k_{-1}/2k_1k_2)[AcrH_2]^{-1} + (2k_1)^{-1} \quad (7)$$

The intercept corresponds to the disproportionation rate constant $(2k_1)^{-1}$. As expected, no kinetic deuterium isotope effect is observed for k_1 (Figure 3b). In contrast, there is kinetic deuterium isotope effect ($k_H/k_D = 2.3 \pm 0.1$) for the rate constant of hydride transfer from $AcrH_2$ and $AcrD_2$ to [(TMP)Mn^{V}(O)]$^+$ (k_2) in the slope of the linear plot; the slope corresponds to $k_{-1}/(2k_1k_2)$.

When $AcrH_2$ is replaced by other NADH analogs shown in Chart 1, the rate of formation of (TMP)Mn^{III}(OH) also obeys second-order kinetics and the k_{obs} value exhibits a saturation behavior (Figure 4a). Virtually, the same k_1 value [(8.0 ± 0.6) × 10^6 M^{-1} s^{-1}] was obtained from the identical intercepts of the plots in Figure 4b. Thus, it was confirmed that the disproportionation rate constant (k_1) remained the same irrespective of the difference in substrates. The k_1 and k_2K_1 ($K_1 = k_1/k_{-1}$) values are summarized in Table 1. According to Scheme 2, the disproportionation rate constant (k_1) should increase with increasing the proton concentration. This was confirmed in Figure 5, where the dependence of k_{obs} on [$AcrH_2$] is plotted with different concentrations of *m*-CPBA. The derived k_1 value increases linearly with increasing concentration of *m*-CPBA.

Table 1. Rate Constants (k_2K_1) of Hydride Transfer from NADH Analogs to (TMP)Mn^{IV}(O) and Rate Constants (k_1) of Disproportionation of (TMP)Mn^{IV}(O) in MeCN at 298 K

NADH analog	k_2K_1, M^{-2} s^{-1}	k_1, M^{-1} s^{-1}
BNAH	(2.3 ± 0.2) × 10^9	(7.0 ± 0.4) × 10^6
$AcrH_2$	(4.2 ± 0.3) × 10^8	(8.0 ± 0.6) × 10^6
$AcrD_2$	(1.8 ± 0.1) × 10^8	(9.0 ± 0.7) × 10^6
AcrHMe	(3.3 ± 0.2) × 10^8	(9.0 ± 0.8) × 10^6
AcrHPh	(9.0 ± 1.0) × 10^6	(7.0 ± 0.5) × 10^6

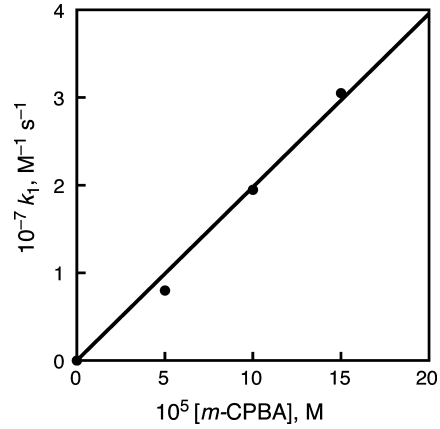

Figure 5. Plot of k_1 vs [*m*-CPBA] for hydride transfer from $AcrH_2$ to (TMP)Mn^{IV}(O) in the presence of different concentrations of *m*-CPBA.

Comparison of the Hydride-Transfer Reactivities of (TMP)Mn^{IV}(O) vs *p*-Chloranil. The rate constants of hydride transfer from NADH analogs to (TMP)Mn^{IV}(O) are compared with those of hydride transfer from the same series of NADH analogs to *p*-chloranil (Cl_4Q) (see SI, Table S1).[15b] There is a good linear correlation recognized between the log k_2K_1 values of (TMP)Mn^{IV}(O) and the corresponding values (k_H) of Cl_4Q as shown in Figure 6. In each case, a significant decrease in the reactivity is recognized by the introduction of a substituent R at the C-9 position of $AcrH_2$. This can hardly be reconciled by a one-step hydride-transfer mechanism. The alkyl or phenyl

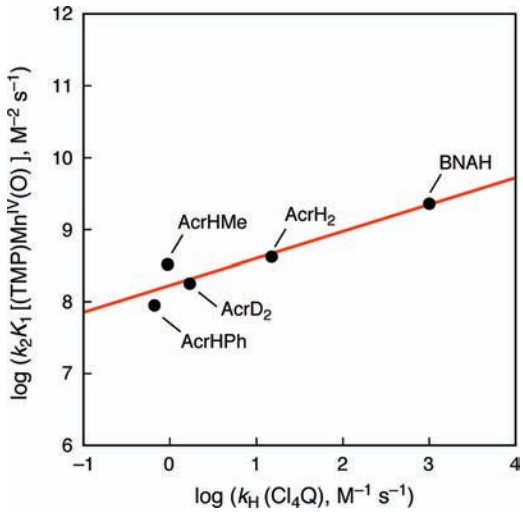

Figure 6. Plots of k_H or k_2K_1 for hydride transfer from NADH analogs to (TMP)Mn^{IV}(O) vs k_H for hydride transfer from the same series of NADH analogs to Cl_4Q in MeCN at 298 K.

group at the C-9 position is known to be in a boat axial conformation, and thereby the hydrogen at the C-9 position is located at the equatorial position, where steric hindrance due to the axial substituent is minimized in the hydride transfer reactions. The introduction of an electron-donating substituent R would activate the release of a negatively charged hydride ion if the concerted hydride transfer should take place. The remarkable decrease in the reactivity with the increasing electron-donor ability of R rather indicates that the reactivity is determined by the process in which a positive charge is released.

Electron Transfer from Ferrocene Derivatives to (TMP)Mn^{IV}(O). When a one-electron reductant such as ferrocene (Fc) is employed as a substrate, electron transfer from Fc to (TMP)Mn^{IV}(O) occurs to produce ferricenium ion (Fc^+) and (TMP)Mn^{III}(OH) (eq 8; Figure 7a). The 1:1 stoichiometry was confirmed by the spectral titration (Figure 7b).

$$\text{(TMP)Mn}^{IV}\text{(O)} + \text{Fc} + \text{H}^+ \rightarrow \text{(TMP)Mn}^{III}\text{(OH)} + \text{Fc}^+ \quad (8)$$

The rate of formation of (TMP)Mn^{III}(OH) obeys first-order kinetics rather than second-order kinetics (Figure 8a), which is in sharp contrast to the cases of $AcrH_2$ and AcrHPh described above. The pseudofirst-order rate constant (k_{obs}) increases linearly with increasing concentration of Fc, and the second-order rate constant of electron transfer from Fc to (TMP)Mn^{IV}(O) is determined to be 1.6×10^5 M^{-1} s^{-1} (Figure 8b). The rate constant of electron transfer from Fc to (TMP)Mn^{IV}(O) remains constant irrespective of the acid concentration (see SI, Figure S3).

Electron transfer from a series of ferrocene derivatives to (TMP)Mn^{IV}(O) was also examined to determine the reorganization energy of electron transfer (see SI, Figure S4). The k_{et} values are listed in Table 2 together with the one-electron oxidation potentials of ferrocene derivatives.[15a] The k_{et} value increases with decreasing the E_{ox} value.

The driving force of electron transfer from ferrocene derivatives to (TMP)Mn^{IV}(O) is determined by eq 9,

$$-\Delta G_{et} = e(E_{red} - E_{ox}) \quad (9)$$

where E_{ox} is the one-electron oxidation potentials of ferrocene derivatives[15a,21] and E_{red} is the one-electron reduction potential of (TMP)Mn^{IV}(O). The E_{red} value of (TMP)Mn^{IV}(O) was determined to be 0.59 V vs SCE using differential pulse voltammetry (see SI, Figure S5).

The dependence of the k_{et} value on the ΔG_{et} value for outer-sphere electron transfer has been well established by Marcus as given by eq 10,

$$k_{et} = Z\exp[-(\lambda/4)(1 + \Delta G_{et}/\lambda)^2/k_BT] \quad (10)$$

where λ is the reorganization energy of electron transfer, k_B is the Boltzmann constant and Z is the collision frequency taken as 1×10^{11} M^{-1} s^{-1}, and T is the absolute temperature.[14] Then, the λ value is determined using eq 11, which is derived from eq 10.

$$\lambda = -\Delta G_{et} - 2RT\ln(k_{et}/Z) + [\{\Delta G_{et} + 2k_BT\ln(k_{et}/Z)\}^2 - (\Delta G_{et})^2]^{1/2} \quad (11)$$

Virtually the same λ values are obtained irrespective of the difference in the driving force as shown in Table 2. The λ value of the electron-transfer reduction of (TMP)Mn^{IV}(O) (avg. 1.71 $\pm$ 0.09 eV) is significantly smaller than the values of the electron-transfer reduction of nonheme iron(IV)−oxo complexes [(L)Fe^{IV}(O)]$^{2+}$ (L = TMC, 1,4,8,11-tetramethyl-1,4,8,11-tetraazacyclotetradecane: 2.37 eV; Bn-TPEN: 2.55 eV; N4Py: 2.74 eV).[15a]

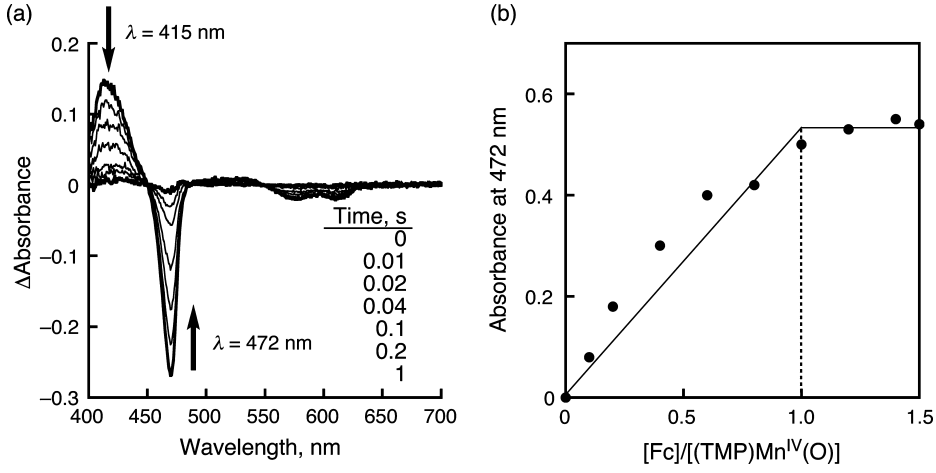

Figure 7. (a) UV−vis spectral change observed in electron transfer from Fc (3.0×10^{-4} M) to (TMP)Mn^{IV}(O) (5.0×10^{-6} M) in MeCN at 298 K. Note that the different spectra were taken in reference to that after the reaction. (b) Spectral titration of the stoichiometry of the electron-transfer reactions.

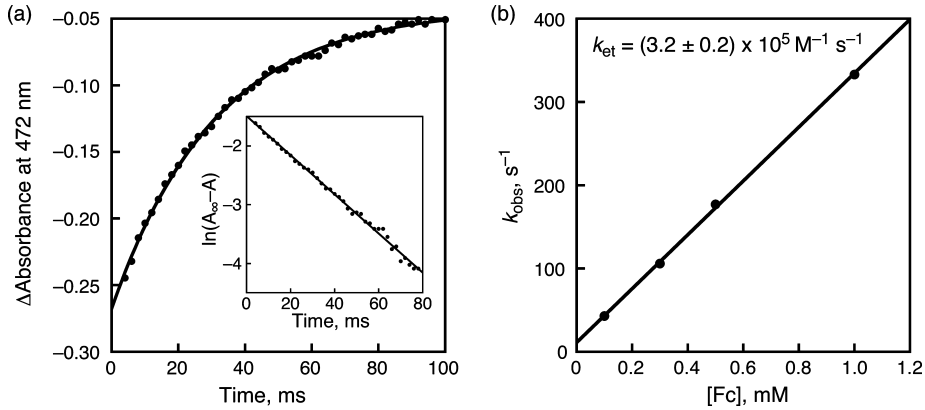

Figure 8. Time profile of the absorption change at $\lambda = 472$ nm in electron transfer from Fc (1.0×10^{-4} M) to (TMP)Mn^{IV}(O) (5.0×10^{-6} M). (Inset) First-order plot. (b) Plot of k_{obs} vs [Fc].

Table 2. Oxidation Potentials (E_{ox}) of Ferrocene Derivatives, Rate Constants (k_{et}) and Reorganization Energies (λ) for Electron Transfer from Ferrocene Derivatives to (TMP)Mn^{IV}(O) in MeCN at 298 K

ferrocene derivative	E_{ox},[a] V vs SCE	k_{et}, M^{-1} s^{-1}	λ, eV
Me_2Fc	0.26	$(9.2 \pm 0.9) \times 10^5$	1.80 ± 0.10
Fc	0.37	$(3.2 \pm 0.2) \times 10^5$	1.72 ± 0.09
BrFc	0.54	$(4.3 \pm 0.3) \times 10^4$	1.62 ± 0.07

[a] Taken from ref 15a.

We have shown above that hydride-transfer reactions of NADH analogs with (TMP)Mn^{IV}(O) occurs via disproportionation of (TMP)Mn^{IV}(O) to produce $[(TMP)Mn^{III}]^+$ and $[(TMP)Mn^{V}(O)]^+$ that is the actual hydride acceptor, whereas electron transfer from Fc to (TMP)Mn^{IV}(O) occurs directly without involvement of the disproportionation (Scheme 3). Thus, (TMP)Mn^{IV}(O) acts only as one-electron oxidant in the latter reaction. The apparent reactivity of (TMP)Mn^{IV}(O) as a two-electron oxidant results from the disproportionation to produce a two-electron oxidant, $[(TMP)Mn^{V}(O)]^+$. However, electron transfer from ferrocene derivatives to $[(TMP)Mn^{V}(O)]^+$ may also be much faster than the electron transfer to (TMP)Mn^{IV}(O). The observation of direct electron transfer from ferrocene derivatives to (TMP)Mn^{IV}(O) rather than the electron transfer to $[(TMP)Mn^{V}(O)]^+$ may be ascribed to the disfavored disproportionation equilibrium (vide supra).

Mn(V) porphyrins have been prepared as a stable form in the presence of a base,[6,7] which is shown to be *trans*-dioxomanganese(V) species [O═Mn^{V}═O].[6d] Hydride transfer from NADH analogs to *trans*-dioxomanganese(V) porphyrin complexes was reported to occur, producing the corresponding manganese(III) complexes.[7c] The rate constant of hydride transfer from $AcrH_2$ to a *trans*-dioxomanganese(V) complex ([(TPFPP)$Mn^{V}(O)_2$]: TPFPP = 5,10,15,20-tetrakis(pentafluorophenyl)porphyrin) was determined to be 15 M^{-1} s^{-1} in the presence of a base (tetra-*n*-butylammonium hydroxide) in a solvent mixture of MeCN and CH_2Cl_2 (1:1) at 298 K.[7c] This is much slower than the rate of hydride transfer from $AcrH_2$ to (TMP)Mn^{IV}(O), which proceeds via the rate-determining disproportionation with the rate constant of $(8.0 \pm 0.6) \times 10^6$ M^{-1} s^{-1} (vide supra). This indicates that *trans*-dioxomanganese(V) porphyrin complexes, which are formed in the presence of a base, are much less reactive than $[(TMP)Mn^{V}(O)]^+$, which is produced via disproportionation of (TMP)Mn^{IV}(O) in the presence of an acid.

Conclusion

The observations of the second-order kinetics in hydride-transfer reactions of NADH analogs with (TMP)Mn^{IV}(O) and the dependence of the observed second-order rate constants on concentrations of NADH analogs clearly indicate that the hydride transfer proceeds via the rate-determining disproportionation of (TMP)Mn^{IV}(O) to $[(TMP)Mn^{III}]^+$ and $[(TMP)Mn^{V}(O)]^+$, followed by fast hydride transfer from NADH analogs to $[(TMP)Mn^{V}(O)]^+$ in competition with the comproportionation back to $[(TMP)Mn^{III}]^+$. NADH analogs that are two-electron reductants can only react with $[(TMP)Mn^{V}(O)]^+$ to produce the corresponding NAD^+ analogs and [(TMP)Mn^{III}(OH)]. In contrast to the two-electron reductants, ferrocene derivatives that are one-electron reductants react directly with (TMP)Mn^{IV}(O) by electron transfer. The disproportionation pathway is neglected in electron-transfer reactions because of the unfavorable disproportionation equilibrium. In conclusion, the present study provides valuable mechanistic insights into the change of reaction pathways depending on substrates and reaction conditions; that is, (TMP)Mn^{IV}(O) is converted to $[(Porp)Mn^{V}(O)]^+$ through disproportionation process in hydride-transfer reactions, whereas (TMP)Mn^{IV}(O) is directly involved in electron-transfer reactions. Our finding of the occurrence of disproportionation of (TMP)Mn^{IV}(O) will make it possible to develop the electron-transfer catalytic oxygenation of substrates with one-electron

Scheme 3

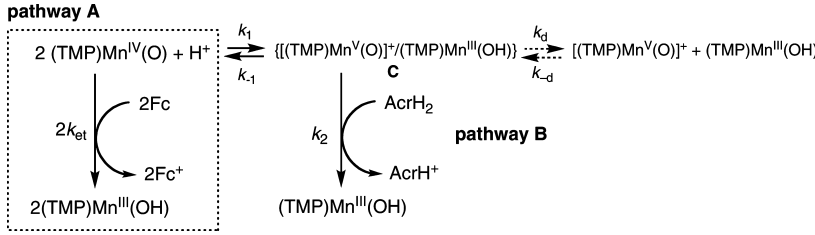

oxidants instead of two-electron oxidants, because the one-electron oxidation of (TMP)Mn^{III}(OH) leads to form the two-electron oxidized species, $[(TMP)Mn^{V}(O)]^{+}$, which is much more reactive than (TMP)Mn^{IV}(O). Such studies on the catalytic oxygenation of a series of substrates with one-electron oxidants by utilizing the disproportionation are now in progress.

Acknowledgment. This work was supported by a Grant-in-Aid (Nos. 19205019, 19750034, 21750146 to S.F. and K.O.) and a Global COE program, "the Global Education and Research Center for Bio-Environmental Chemistry" from the Ministry of Education, Culture, Sports, Science and Technology, Japan, the Korea Science and Engineering Foundation through the Creative Research Initiatives Program (to W.N.), and KOSEF/MEST through WCU project (R31-2008-000-10010-0) (to S.F. and W.N.).

Supporting Information Available: Spectral change for formation of (TMP)Mn^{IV}(O) (S1, Figure S1), ESR spectrum of (TMP)Mn^{IV}(O) (S2, Figure S2), derivation of eq 5 (S3), Table of rate constants (S4, Table S1), plot of k_{et} vs concentration of *m*-CPBA (S5, Figure S3), plots of k_{obs} vs concentrations of ferrocene derivatives (S6, Figure S4), DPV of (TMP)Mn^{IV}(O) (S7, Figure S5). This material is available free of charge via the Internet at http://pubs.acs.org.

JA9045235